Volume 1 | Number 1 | Jan 2013 | Pages 1–100

PCCP

Physical Chemistry Chemical Physics
www.rsc.org/pccp

ROYAL SOCIETY OF CHEMISTRY

ROYAL SOCIETY OF CHEMISTRY

www.rsc.org/pccp

Fullerenes generated from porous structures[†]

Ricardo Paupitz,[*a] **Chad E. Junkermeier,**[b] **Adri C. T. van Duin**[b] **and Paulo S. Branicio**[c]

A class of macromolecules based on the architecture of the well-known fullerenes is theoretically investigated. The building blocks used to geometrically construct these molecules are the two dimensional structures: porous graphene and biphenylene-carbon. Density functional-based tight binding methods as well as reactive molecular dynamics methods are applied to study the electronic and structural properties of these molecules. Our calculations predict that these structures can be stable up to temperatures of 2500K. The atomization energies of carbon structures are predicted to be in the range 0.45 eV/atom to 12.11 eV/atom (values relative to the C60 fullerene), while the hexagonal boron nitride analogues have atomization energies between -0.17 eV/atom and 12.01 eV/atom (compared to the B12N12 fullerene). Due to their high porosity, these structures may be good candidates for gas storage and/or molecular encapsulation.

1 Introduction

In the last few decades materials scientists have thoroughly investigated the properties of many carbon-based structures. This quest resulted in the experimental verification of fullerenes[1], carbon nanotubes (CNT)[2], and graphene[3,4]. Further effort has been put into understanding changes in the mechanical, electrical, and chemical properties due to defects[5], adsorbates[6–9], and electromagnetic fields[10], for instance. Also, the synthesis of these carbon based materials has led to great interest into inorganic analogues, such as silicene[11,12], germanene, and hexagonal boron nitride[13](hBN) which are respectively the silicon-based, germanium-based, and boron nitride analogues of graphene. In this context, the latter is of special interest, due to the fact that the hBN presents the same honeycomb morphology, with almost identical bond lengths and cell parameters as its carbon counterpart. These similarities point to the possibility of synthesis of several boron nitrite nanostructures equivalent to known carbon nanostructures[14–17]. Although these compounds are geometrically similar, their electronic properties are quite different leading to interesting contrasts, for instance the zero-width band gap of graphene compared to the wide band gap of hBN. Taking into account these interesting facts, we included in the present study not only carbon-based structures, but also their hBN counterparts.

Theoretical works have proposed super structures, based on fullerene[18,19], nanotube[20] or graphene[21] architectures. These superstructures often mimic the pattern of one of the well-known carbon allotropes but use another structure as the building blocks. For example, Coluci *et al.* use single walled CNT linked together with y-like junctions to form a super nanotube[20]. These structures can present interesting properties, for instance mechanical stability at high temperatures, and can be promising alternatives in the development of highly porous, flexible, and high strength materials. Calculations regarding the electronic properties of some of these materials have shown the possibility of metallic or semiconducting behavior depending on the specific construction of the superstructure[22].

Well before the experimental verification of graphene, theorists were predicting alternative two-dimensional carbon structures. These structures have the potential to overcome some of the inherent limitations of graphene (i.e. zero band gap). Baughman *et al.* studied many such structures comparing their mechanical properties and formation energies, predicting that graphyne (also called 6,6,6-graphyne or γ-graphyne) would be one of the easiest to synthesize[23]. Recently, a new synthesis route, using dehydrogenation of porous graphene, suggested that biphenylene-carbon (BPC) could be synthesized conveniently as well[24,25].

Alternatively, the discovery of the C60 molecule generated a tremendous expectation that new materials with novel properties could be synthesized with fullerene like structures as a building unit. However, the synthesis of these strucures has always been challenging. Nonetheless, steady progress has been made on the identification of synthesis routes for closed cage structures, e.g. fullerenes and heterofullerenes. Ray *et al.* reported the synthesis of silicon-doped heterofullerenes in the carbon-rich limit based on quenching of SiC plasma, generated by laser vaporization, with a high pressure helium burst promoting SiC heterofullerenes growth and ejection[26]. Hulman *et al.* reported the generation of CN aza-fullerenes consisting of cross-linked nano-onions of C
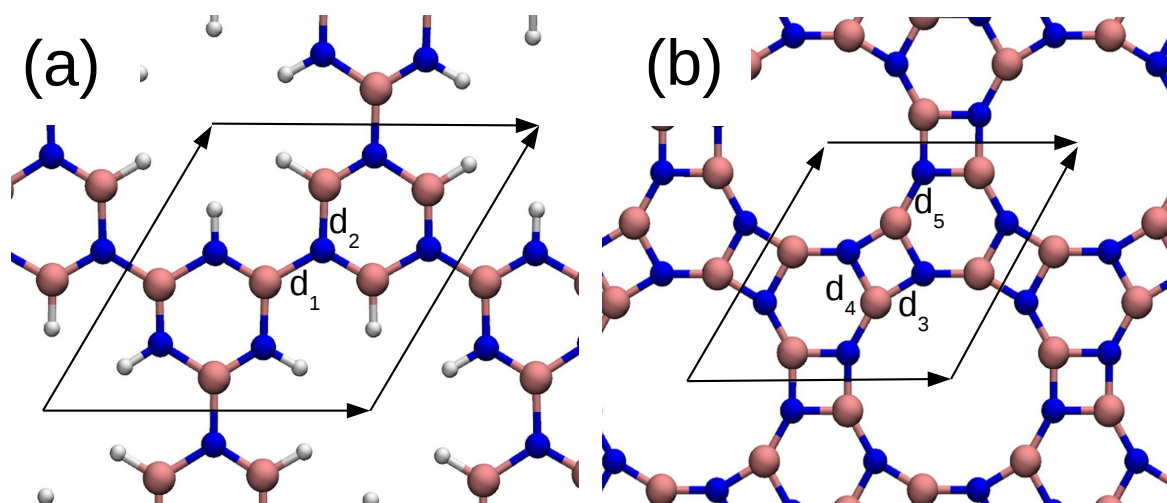
Fig. 1 (a) Bond definitions for porous-type structures, carbon-hydrogen distances will be indicated by d_{CH}, boron-hydrogen by d_{BH} and nitrogen-hydrogen by d_{NH} in the text. Blue circles represent nitrogen atoms, pink circles represent boron atoms and the white ones represent hydrogen atoms. For carbon structures, both, blue and pink circles would represent carbon atoms, while white still represents hydrogen. (b) Bond numbers for Biphenylene-type structures.

and N by magnetron sputtering[27]. Narita *et al.* reported the synthesis of hBN fullerenes by an arc-melting of a combination of B rich metal powders and catalysis metals (Nb, Y, and Sc) in a N_2/Ar atmosphere[28]. Nakamura *et al.* reported the synthesis of heterofullerenes by direct hBN substitution reaction of C_{60} under irradiation with a KrF excimer laser[29]. Melinon *et al.* discussed the theoretical principles and the experimental work on SiC cage-like clusters[30]. Recently, the use of a laser-vaporization cluster source to achieve the synthesis of the all-boron fullerene[31], namely B_{40}, was reported by Zhai *et al*. The use of heated metallic surfaces to promote dehydrogenation of aromatic precursors as an alternative route for the generation of fullerene structures was also reported[32]. The identification of these new synthesis routes point to the need to investigate theoretically the structures and superstructures created out from BPC and related building blocks.

Using a combination of density functional tight binding methodology (DFTB)[33] and a reactive force field[34] we investigate the electronic and structural properties of the closed shell molecules based on the architectures of well known fullerenes in which the building blocks are the unit cells of porous graphene and BPC, as well as their hBN structural analogs[35]. The porous graphene and BPC units cells are shown in Figure 1. As a starting point we used the architectures of some of the simplest fullerenes found in literature[1,36], these are C20, C24, C36, C48 and C60, shown in the first row of Table 1. For each carbon-carbon bond in one of these structures we substituted one of the unit cells shown in the first column of Table 1, we were able to construct several "closed shell" molecules. These unit cells were chosen for their symmetry and for the fact that each one was either predicted and/or already synthesized in two-dimensional sheets. Some of these structures were already proposed elsewhere[37]. The porous hBN analogs of C20 and C60 resulted in systems that had B-B or N-N bonds and were thus not included in this work since their geometry preclude consistent closed shell construction. The considered structures and architectures are shown in Table 1. The second and third rows are fullerenes based on porous graphene and graphenylene[38], while the last two rows contain the hBN analogues, porous hBN and inorganic graphenylene[39]. Each molecule was then optimized, the electronic properties computed, and an estimate of the range in temperature at which they are stable in the gas phase was produced.

[a] Departamento de Física, IGCE, Univ Estadual Paulista, UNESP, 13506-900, Rio Claro, SP, Brazil; Tel: 55 019 3526 9156; E-mail: paupitz@rc.unesp.br

[b] Department of Mechanical and Nuclear Engineering, The Pennsylvania State University, University Park, PA 16802, USA

[c] Institute of High Performance Computing, 1 Fusionopolis Way, #16-16 Connexis, Singapore 138632, Singapore

	C20	C24	C36	C48	C60
Legend Picture symmetry group LUMO–HOMO [eV] Linear Break [K] Stepped Break [K]	Ih 0.73 3301	Oh 1.67 1810	D3h 0.89 1569	Oh 0.87 2412	Ih 1.19 4193
	Ih 3.38 2729 2759	Oh 2.91 2668 2700	C1 3.00 2638 2400	Oh 2.88 2579 2446	C2 3.11 2709 2761
	Ih 1.63 1304 1261	Oh 0.81 1273 1200	D3h 0.01 1241 1200	Oh 0.70 1275 1288	Ih 1.19 1203 1200
	X	Th 4.24 1427 1400	D3 4.22 1403 1292	O 4.18 1358 1300	X
	I 3.69 814 700	O 3.51 910 900	D3 3.51 1052 967	O 3.52 996 800	I 3.32 853 753
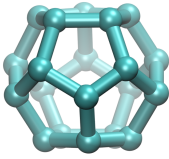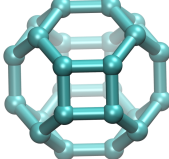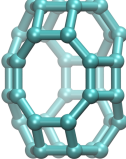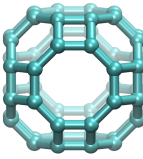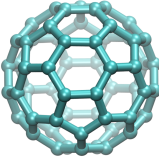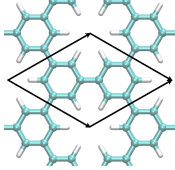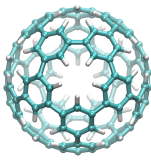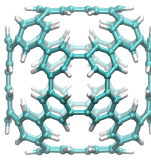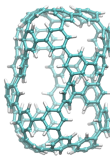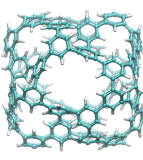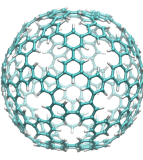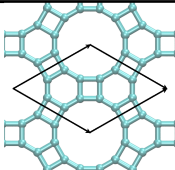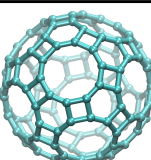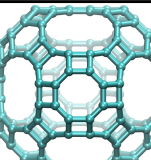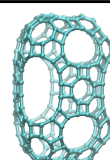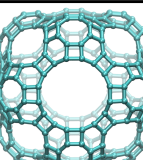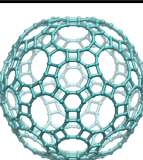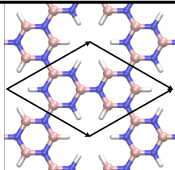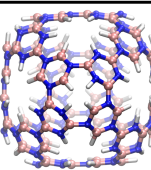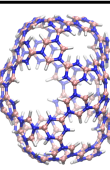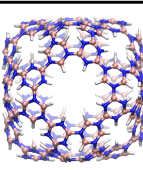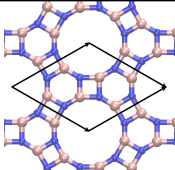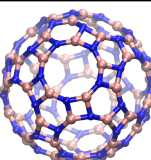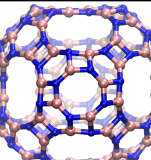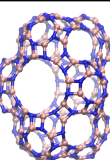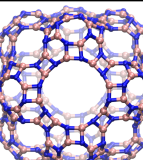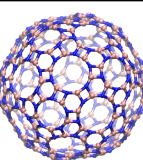
Table 1 Architectures considered in this work are indicated in the first row. The repeating units used for each one of the molecules considering the respective architecture are indicated in the first column. The "**X**" symbols indicate structures which are not possible to construct using the hBN repeating units. Symmetry groups, band gaps, and breaking temperatures are indicated for each one of the considered architectures.

2 Methodology

Geometry optimizations and electronic structure calculations of all the molecules in Figure 1 were performed using DFTB in its self consistent charge (SCC)-DFTB version as implemented in the DFTB+ code[33]. DFTB methodology was conceived to benefit from both the low computational cost of tight binding methods and of the DFT capability to describe a wide range of phenomena for several classes of molecules and compounds[40]. This methodology is based in a second-order expansion of the Kohn-Sham energy defined in DFT and has been used successfully to describe a great variety of systems which include organic molecules, hydrocarbons, and systems of interest for materials scientists, such as solids and surfaces[33,41]. It is known that energy and gap values obtained with this methodology usually are underestimated, since it considers only valence electrons[42]. For this reason, DFTB+ is particularly useful when the interest is to obtain relative energy values or to explain trends in a series of large atomic structures. The particular parameterization used in the present work was already tested in other systems of interest for materials sciences[43]. In the case of geometry optimizations, a nonperiodic system was considered and a conjugate gradient algorithm applied during the search for the minimal energy configuration. As convergence criteria for the geometrical search and for the SCC iterations we adopted a maximum force difference of 10^{-5} and a maximum tolerance of 10^{-4} respectively.

Since our interest was to understand the behavior of these molecules with respect to temperature, a stability study was performed using ReaxFF[34]. ReaxFF is a reactive force field method developed by van Duin, Goddard III and co-workers which allows the calculation of chemical reactions[44,45]. ReaxFF has some characteristics that are similar to those found in standard non-reactive force fields. In non-reactive force fields, the system energy is divided into partial energy contributions associated valence angle, bond stretching, bending as well as non-bonded van der Waals and Coulomb interactions as, for instance, in the MM3 force field[46,47]. In the case of ReaxFF, it is possible to describe bond formation and dissociation (making/breaking bonds) as a function of bond order values. ReaxFF parameters are optimized against DFT calculations and have been widely used in the description of large systems up to a billion atoms.[48] In this work we used an established reactive force field parameterization for carbon[45] and a newly developed parameterization for boron nitride (BN).

To generate a ReaxFF H/C/B/N force field capable of simulating B/N containing fullerenes we extended the ReaxFF C/H/O description from Chenoweth *et al.* [45] with B/C, B/N bond parameters with associated angle and dihedral parameters. These new parameters were trained against a DFT-based training set, consisting of the previously employed aminoborane dehydrogenation and combustion training set[49], extended with DFT data describing the variation of the cohesive energy and heats of formation as a function of volume for BN-crystals in the hexagonal (hBN), zinc blend (zBN), and wurtzite (wBN) structures. Figure 2 compares the atomization energies for these phases and the equations of state for the BN phases from both ReaxFF and DFT indicating that ReaxFF provides a good description of both the mechanical properties as well as the thermodynamic stability of these BN condensed phases.

Using the DFTB+ optimized structures as the starting point, we first relaxed each structure in Reaxff before running the molecular dynamics (MD) calculations. All MD calculations were performed using a velocity Verlet algorithm with a time step of 0.25 fs in the canonical ensemble (NVT), the Berendsen-Anderson temperature damping constant is 2.5 fs. We use the Reaxff optimized structures as the starting configurations for NVE calculations at 10 K for 100,000 time steps from which we pull out ten structures, each at a temporal separation of 10,000 time steps and used each of them as a starting configuration for a temperature ramp calculation. Two types of temperature ramps were performed on each structure. The first temperature ramp is a linear increase from 10 K to 300 K at a rate of 0.001 K per time step and then at a rate of 0.002 K per time step from 300 K to 3700 K. The second temperature ramp is a stepped increased that first went linearly from 10 K to 600 K, then starting at 600 K alternated running at a constant temperature for 50,000 time steps and then increased linearly at a rate of 0.002 K for 50,000 time steps up to a temperature of 3000 K. Thus a total of 360 (180 linear and 180 stepped) temperature ramp calculations were performed. In order to investigate the possibility of an encapsulation capability of these new molecules, we also used ReaxFF methodology as implemented in LAMMPS[50] software to perform molecular dynamics calculations considering the presence of diatomic gases in the environment. During these calculations, constant temperatures were considered from 100K up to 600K, also using a Verlet algorithm in the NVT ensemble with a timestep of 0.1 fs for a total simulation time around 30ps. The simulation box was rectangular with dimensions $140Å \times 140Å \times 140Å$ and there were around 500 molecules of the considered gas (H_2 or O_2).

3 Results and Discussion

As we can see in Table 1 some of the symmetrical characteristics of the original architectures are preserved in most of the molecules, despite of the significant geometrical modification revealed by the optimization process. There are similarities between carbon structures and their hBN analogues with the difference that, in molecules containing BPC-type repeating units, the
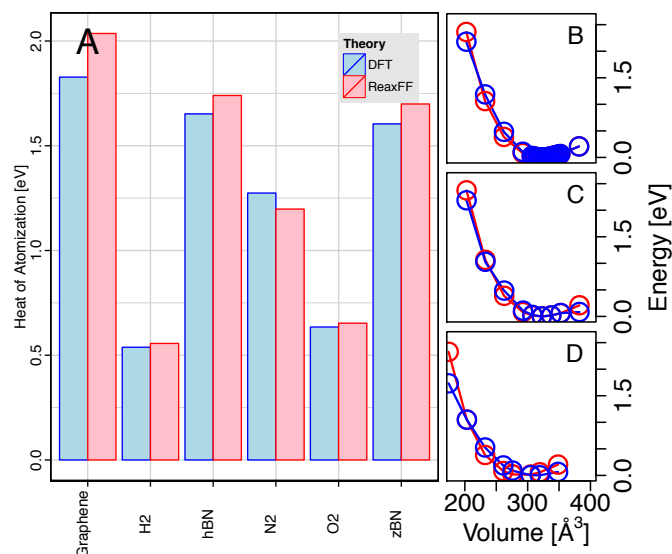
Fig. 2 Comparison of ReaxFF and DFT results in the B/N force field optimization. (A) Heats of atomization for H/B/O/N containing materials. equations of state for B/N condensed phases: (B) zBN (C) wBN (D) hBN.

hBN analogue does not present rectangular motifs, since these are deformed. The C-C and B-N bond lengths (d_1, d_2,..., d_5) as specified in Figure 1 are proportionally different within each molecule, for example d_3:d_4:d_5 in the carbon based BPC analogue of C20 is not equal to d_3:d_4:d_5 in the carbon based BPC analog of C24. The bond-length values of porous carbon structures are (in Å following the nomenclature defined in Figure 1): d_1=1.49Å, d_2=1.41Å and d_{CH}=1.09Å. In hBN porous-like structures, the distances are d_3=1.51Å, d_4=1.46Å, d_{BH}=1.21Å and d_{NH}=1.05Å. The carbon based BPC molecules resulted in d_1=1.48Å when the bond is inside a five-membered pore (with five hexagons as its corners) and d_1=1.51Å, when d_1 refers to a six-membered pore (with six hexagons as corners), d_2=1.48Å while d_3=1.37Å for five-membered and d_3=1.38Å for six-membered pores. The hBN based BPC molecules had d_1=1.50Å for five-membered rings, d_2=1.52Å, for hexagonal rings and d_3=1.44Å. These values are in good agreement with values found in the literature for the 2-dimensional structures (both, porous and BPC) with small deviations as expected since the molecules considered in this work have curvature and closed-cage format.

Table 1 gives the symmetry groups for each one of the template fullerenes and the optimized molecules considered here. Some of them present geometry with the exact same symmetry of the corresponding original fullerene. This happens for instance in the case of C36 architecture using BPC-like repeating unit. This tendency is more pronounced in the BPC based structures (in both the C and BN based molecules). The smaller symmetry of the porous based molecules can be partially understood considering the effect of hydrogen atoms in the structure. Considering the fact that each H atom occupies a finite volume in space and that there is an energetic cost for the overlapping of two electronic densities, in several cases a deformation of the region containing these H bonds is energetically favored. Therefore it is clear that porous structures can have, more easily than BPC structures, several geometrical configurations with similar energy, due to the rearrangements of H atoms. This kind of effect becomes clear in the case of porous-like C36 and C48 molecules, which present symmetries quite different from their templates.

The use of the DFTB Methodology is particularly suitable for the determination of energy differences. In the present case, we estimated the energy difference between frontier orbitals, namely the difference between the highest occupied molecular orbital (HOMO) and the lowest unoccupied molecular orbital (LUMO), dE. The values in Table 1 show that some trends found in two dimensional systems are present, for instance, for structures geometrically related, it is expected that a larger gap between the frontier orbitals of hBN structures than those of the carbon equivalents. For instance, the carbon based porous structures have dE in a range from 2.88 eV to 3.37 eV while the hBN analogs present gaps in the range 4.18 eV to 4.24 eV. Also, in the case of the BPC type fullerenes, we have pure C molecules presenting dE in the range 0.01 eV to 1.6 eV with BPC_{36} presenting the smaller value, while the range turns out to be dE between 3.3 eV to 3.7 eV for BN structures. Another set of differences can be identified in the charge distributions, as shown in Figures 3 and 4. In the case of pure C compounds, the charge distributions are relatively uniform, as one can see in Figure 4a for BPC_{24} and Figure 3c for porous C fullerene. In Figure 3c and 3d, we present plots that indicate with colors (red to negative and blue to positive values) the difference between the calculated total charge density and
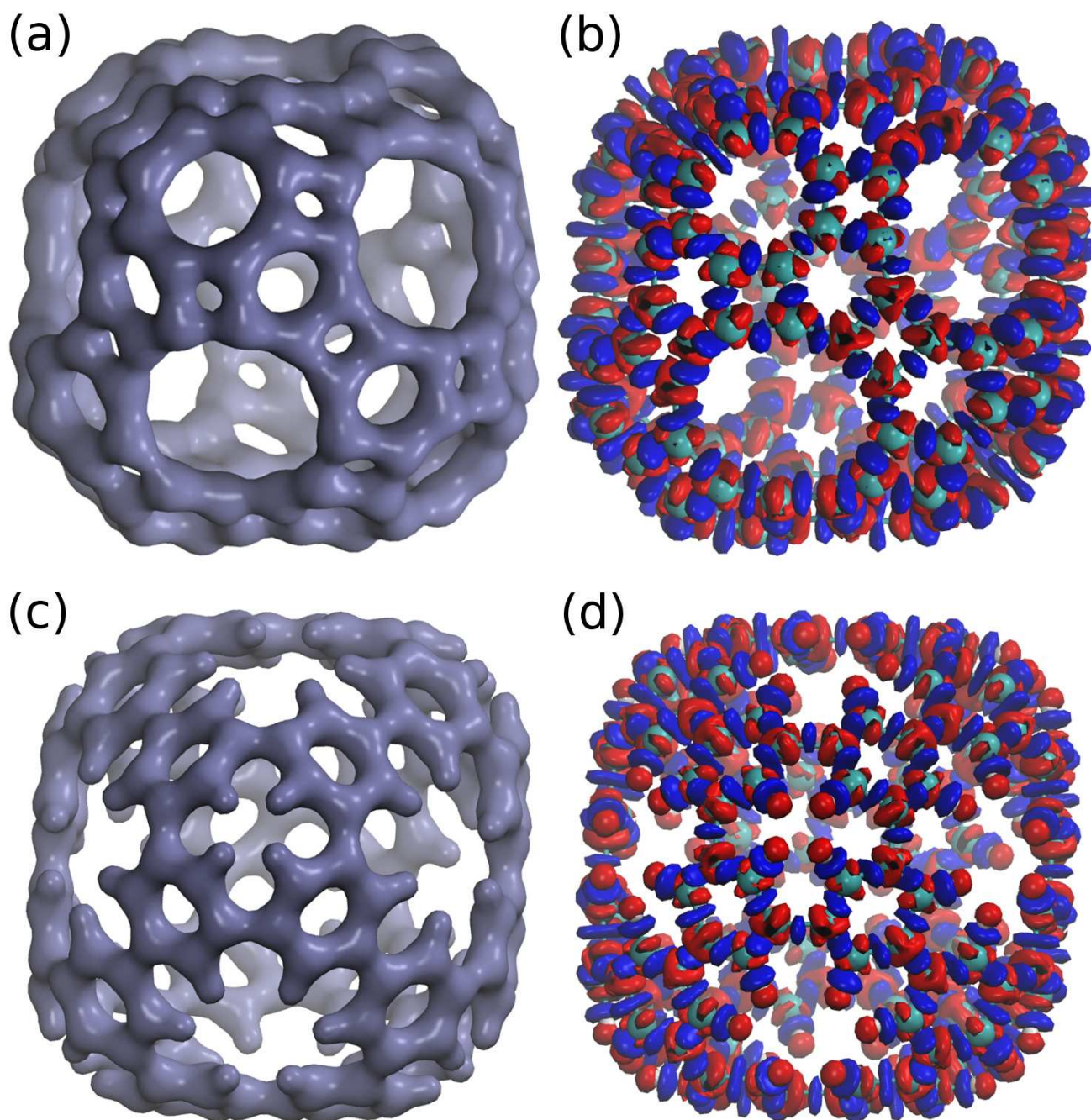
Fig. 3 Charge distribution and charge transference in BPC-24 and porous-24 architectures for carbon-based fullerenes. (a) Charge density distribution for a BPC-24 carbon-based fullerene. (b) Charge differences between calculated charges and the neutral atoms density for a BPC-24 C-based architecture fullerene. (c) Charge density distribution for a porous-24 architecture C based fullerene. Cyan spheres represent carbon atoms, while white represent hydrogen atoms. (d) Charge differences between calculated charges and the neutral atoms density for a porous-24 C-based architecture fullerene.

the density that would be obtained by summing up the densities of the neutral atoms. These plots can be useful to characterize, for example, charge transfers between atoms in the structure. The charges-difference shown in Figure 3b, for the case of BPC_{24} and Figure 3d for the case of porous C fullerene with C24 architecture, indicate a small charge transfer to the region between C atoms, due to the formation of C-C bonds. In contrast, the compounds which contain B and N atoms exhibit charges distributions less uniform (porous BN_{24} - Figures 4a and 4c) while charge variation is shown to be more noticeable in the charge difference graphs (figure 4b and 4d). All the other charge and charge differences distributions for the C and BN compounds can be seen in the Supplementary Materials.

To ascertain the thermal stability of the fullerenes we performed molecular dynamics calculations in which the temperature increases over time to determine the temperature at which the first C-C (or B-N) bond breaks. As stated before, twenty temperature ramp calculations (ten linear increase and 10 stepped increase) were calculated for each structure, we used these to produce descriptive statistics of the temperature at which the first bond was broken. Figure 5 gives the temperatures at which the first bond was broken. There are two box plots for each fullerene structure listed in Table 1, the blue box plots gives the statistical information of the linear increased temperature calculations while the red box plots gives information concerning the stepped increase temperature calculations. The figure shows that the type of material plays the biggest role in when the first bond will likely break. Carbon based BPC (porous) structures break at higher temperatures than the corresponding hBN based BPC (porous) structures, and the porous structures break at higher temperatures than the corresponding BPC structures. In the BPC systems the type-2 bond (as described in Figure 1a) is the first to break 55 percent of the time, while in the porous systems the type-4 bond (as described in Figure 1b) is the first to break 91 percent of the time with the remainder being the type-3 bond (as described in Figure 1b).

The inset of Figure 5 shows the progression of one of the C20 like BPC carbon structures as it undergoes a linear temperature increase. In the BPC structures the breaking of one type-4 bond in a 6-member ring is usually quickly followed by the breaking of one or both of the other type-4 bonds that made up that 6-member ring. Further, up through the temperatures that we probed the BPC structures remained closed molecules and even rehybridized the ring structures at higher temperatures. The porous graphene-like structures, while being more flexible, which allows them to keep their cage structure intact to a much higher temperature, quickly fall apart once the first C-C (B-N) bond is broken.

Taking into account the known fact that CNT are able to encapsulate molecules as well as gases[51–55], it is also reasonable to consider the possibility of trapping gas molecules inside porous fullerenes. In order to investigate this possibility, we performed molecular dynamics calculations for the largest structures considered in the present work, namely the three possible C60 analogs and the porous BN analog of the C48 fullerene. Our preliminary results indicate that due to repulsion between hydrogen atoms located inside the pores and those from the gas, porous carbon structures are less suitable for hydrogen encapsulation than they are for oxygen. Conversely, BPC structures are more suitable for hydrogen trapping since in the case of BPC type molecules the results show that encapsulation was not appreciable for O2 molecules and only significant for H2 at low temperature. On the other hand, with BN structures no reasonable encapsulation was detected. This may be due to the pores on BN fullerenes being either too large (BN porous analog based in C48 architecture) or too deformable (BN BPC type structure based in C60 architecture) precluding an effective encapsulation during the calculations. Our calculations have shown that non bonded interactions (e.g. van der Waals) in conjunction with the closed cage geometry of these molecules create favorable conditions to encapsulate the gas. Further calculations to be presented in a future publication will better clarify these phenomena.

In figure 6(a) and (b), one can see the BPC type carbon structure based in C60 architecture immerse in a H_2 gas, and some of them going inside the structure through the larger pores. In this case, after the first H2s are interacting with the fullerene, some hydrogen molecules go in and some go outside from time to time maintaining always a small number of them inside the cage. The number of H_2 molecules inside the BPC type structure is higher for lower temperatures, this behavior is confirmed by the graph in figure 7(a). In this figure, a comparison between the number of H_2 molecules inside the cage and the average number inside spherical regions of the same size located far from the considered fullerene is presented for two different temperatures, namely 100K and 300K. Higher temperatures were also investigated, up to 600K and there were no significant modifications on the results in comparison to those found for 300K. On the other hand, in figure 6(c) and (d), where the interaction of a porous type structure based in C60 architecture with O_2 molecules is shown, some features are different. In this case, figure 6(d) shows that oxygen molecules are sometimes trapped inside the cage and some of them are blocking the larger pores. The capturing of molecules in the case of porous like fullerenes presents a very different behavior as compared to that found for BPC type structures. As can be seen in figure 7(b), the number of captured molecules grows smoothly throughout the calculations and there is no appreciable influence of temperature on this process.
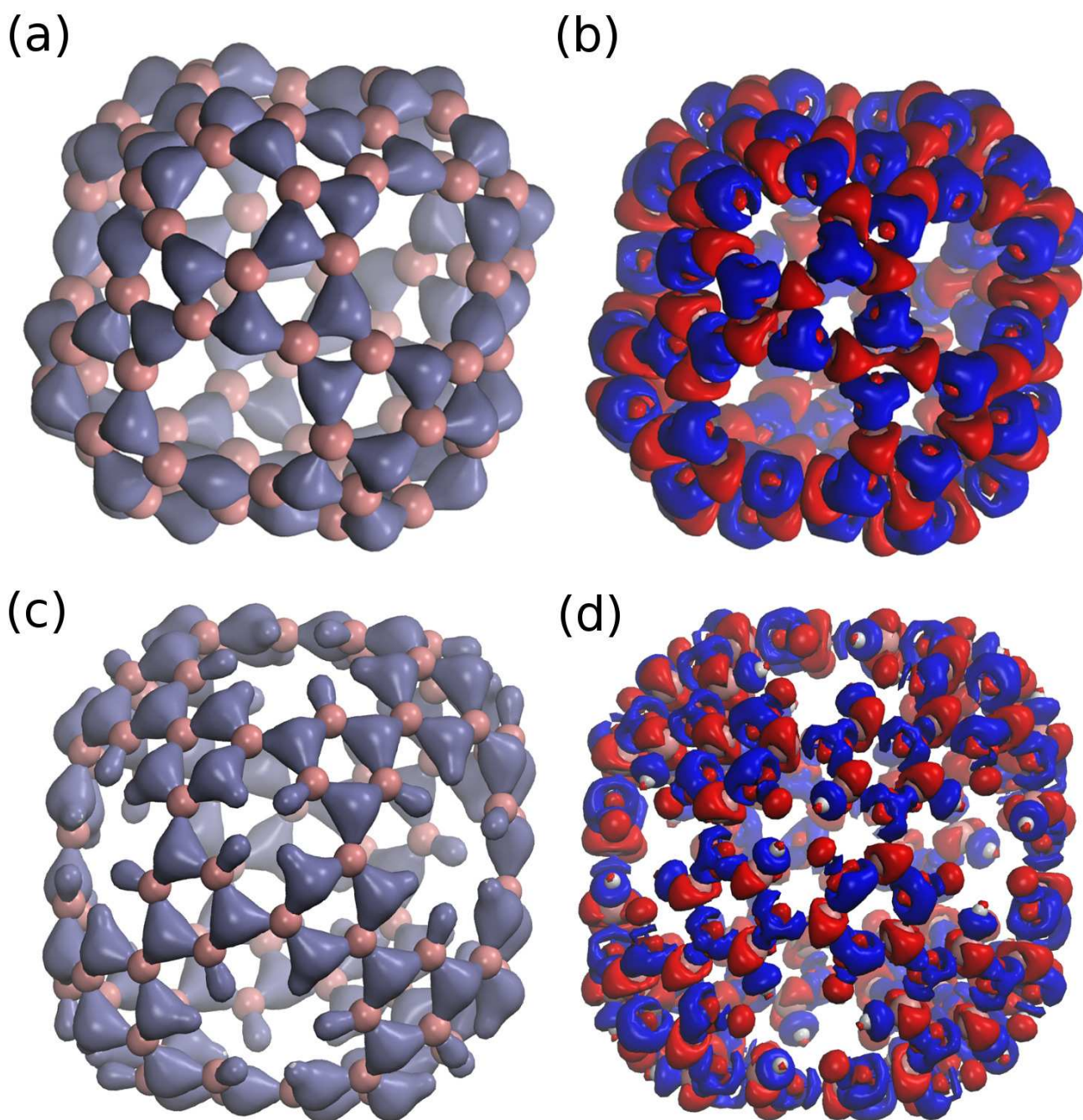
Fig. 4 Charge distribution and charge transference in BPC-24 and porous-24 architectures for hBN-based fullerenes. (a) Charge density distribution for a BPC-24 hBN-based fullerene. (b) Charge differences between actual calculated charges and the neutral atoms density for a BPC-24 hBN-based architecture fullerene. (c) Charge density distribution for a porous-24 architecture hBN based fullerene. Pink spheres represent boron atom while Blue represents nitrogen atoms and white represents hydrogen atoms. (d) Charge differences between actual calculated charges and the neutral atoms density for a porous-24 hBN-based architecture fullerene.
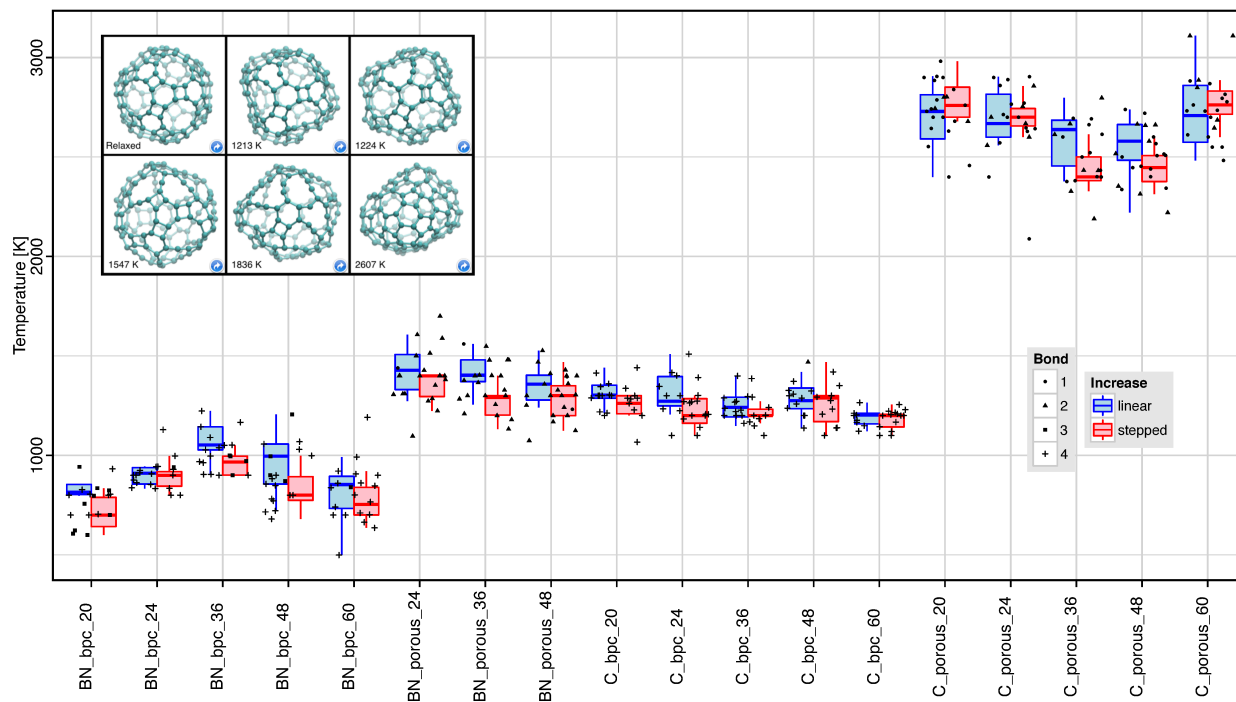
Fig. 5 Boxplot graphs of the temperature at which the first C-C or B-N bond broke in the linear increase (blue bars) or stepped increase (red bars) temperature ramp calculations. The dots represent the calculated values of the C-C (B-N) bond breakage, while the box plots in each column give the extreme of the lower whisker, the lower quartile value, the median value, the upper quartile value and the extreme of the upper whisker.
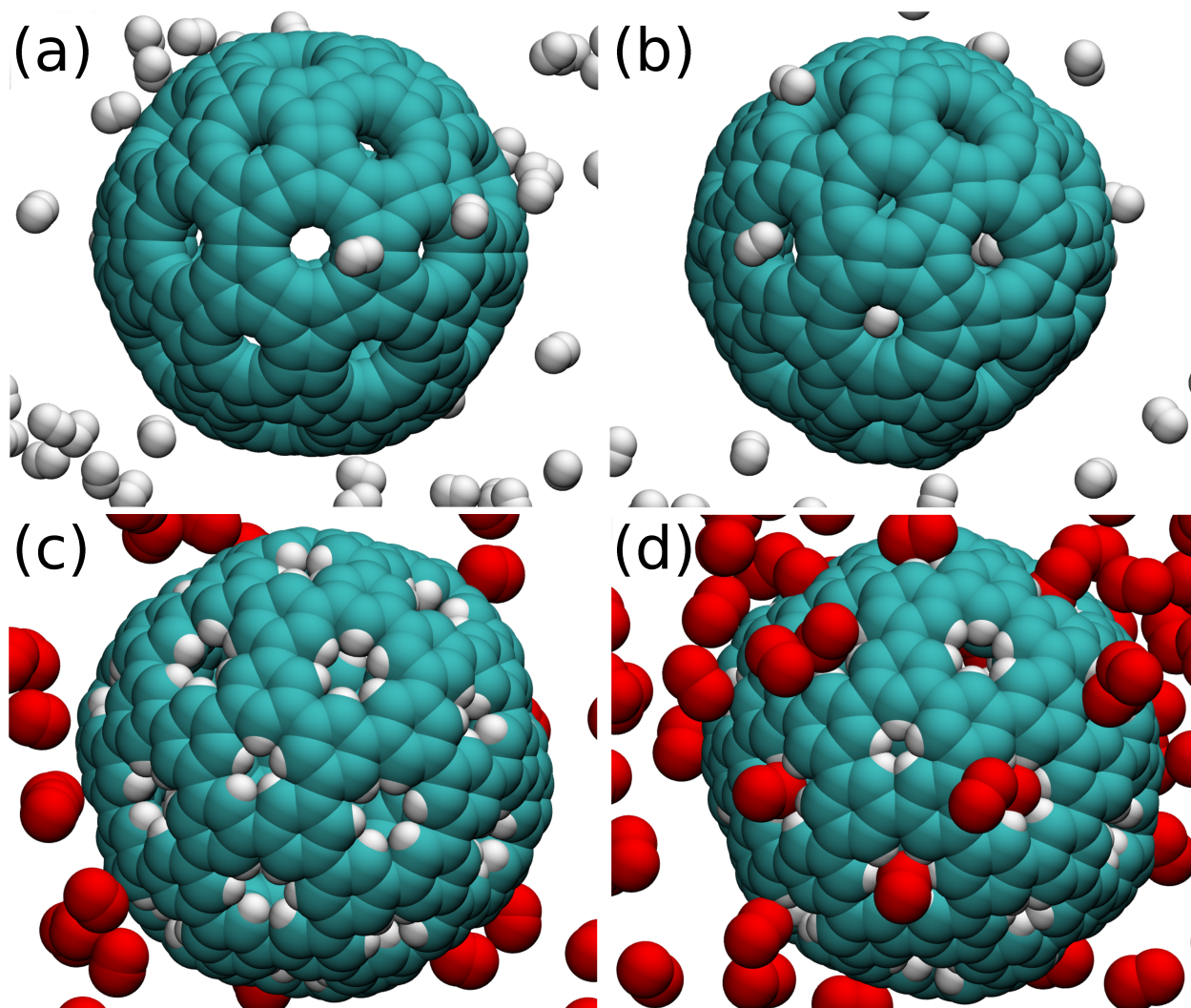
Fig. 6 Fullerenes in gases constituted of O_2 or H_2 molecules at 300K. (a) Shows the initial configuration of molecules of an empty BPC type fullerene with C60 architecture in the beginning of the calculation and (b) The same system after 10 picoseconds when some H_2 molecules lie inside the closed-cage structure respectively. (c) Shows a porous type fullerene with C60 architecture in the beginning of calculation surrounded by O_2 molecules. (d) Shows the system in (c) after 10 ps, when some O_2 molecules were captured and some are inside large pores. Cyan, white and red spheres represent carbon, hydrogen and oxygen atoms respectively.
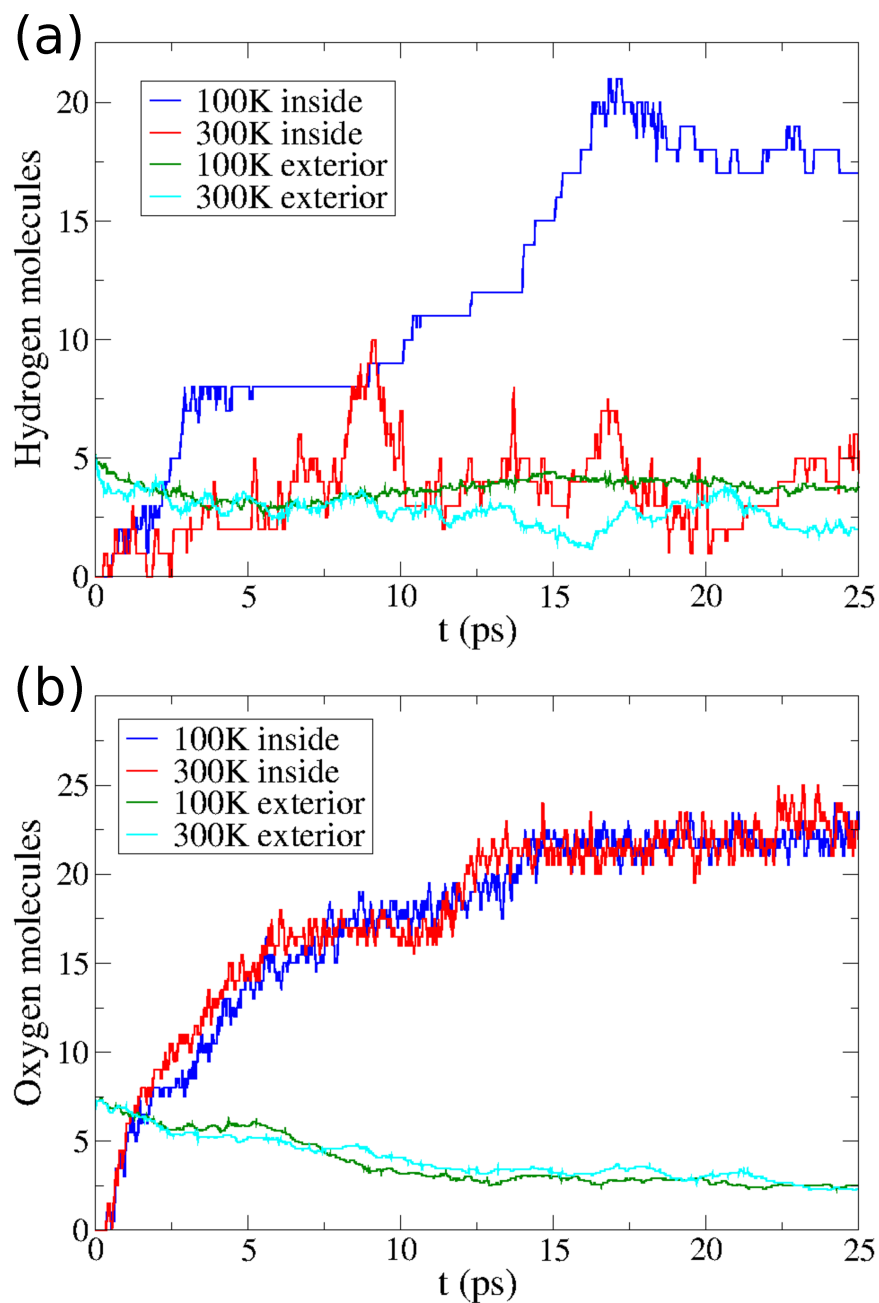
Fig. 7 Comparison between the number of H$_2$ (O$_2$) molecules inside the cage and the average number found in a region far from the considered fullerene. Lines labelled as "inside" indicate the number of molecules inside the molecule, while lines labelled as "exterior" indicate the average number of molecules found in several spherical regions which have the same volume as the considered molecule and are located far from it. (a) Counting for the BPC type fullerene shown in figure 6(a) and 6(b) for temperatures of 100K (blue for inside and green for exterior) and 300K (red for inside and cyan for exterior). (b) Counting of the number of molecules for the porous type fullerene of figure 6(c) and 6(d) for 100K (blue for inside and green for exterior) and 300K (red for inside and cyan for exterior).

4   Conclusion

We have shown the geometrical configuration and demonstrated the thermal stability of 18 molecules that are part of a class of macromolecules based on the architectures of fullerenes and built using either porous graphene or biphenylene-carbon unit cells. In this study, Density functional-based method, DFTB, approach as well as a reactive potential method, ReaxFF, proved to be valuable tools that lead us to important insights in the study of new large molecular systems. Using these two techniques, it was possible to demonstrate that these molecules would maintain their cage-like structure even at higher temperatures, up to $1000K$ for hBN BP-molecules, up to $1200K$ for porous hBN and C-BPC molecules and around $2500K$ in the case of porous-C molecules (figure 5). Two different strategies for molecular heating brought equivalent results for thermal stability. An interesting characteristic found after geometrical optimizations was that, for various molecules, there was a significant geometrical modification if we compare the optimized structure with the original architecture. Despite that, there was a relative preservation of some symmetry characteristics as one can see by comparing the respective symmetry groups in table 1. We have used ReaxFF method to perform molecular dynamics calculations and investigate the possibility of encapsulation of H_2 and O_2 gases by the studied closed-cage structures. Our results show that this is possible to occur, specially in the case of oxygen molecules interacting with porous-type structures and hydrogen inside BPC-like structures. This kind of behavior can be important to gas storage applications in the future and indicates that the encapsulation of gases by these structures should be further investigated. Electronic structure was also investigated and we found a great variation on HOMO-LUMO differences, going from almost 0 eV up to 4 eV in some cases. These can be important to understand chemical interactions with other compounds in future studies.

5   ACKNOWLEDGMENTS

References

1   H. W. Kroto, *Nature*, 1987, **329**, 529–531.

2   S. Iijima, *Nature*, 1991, **354**, 56–58.

3   K. S. Novoselov, A. K. Geim, S. V. Morozov, D. Jiang, Y. Zhang, S. V. Dubonos, I. V. Grigorieva and A. A. Firsov, *Science*, 2004, **306**, 666–669.

4   A. K. Geim and K. S. Novoselov, *Nature Materials*, 2007, **6**, 183–191.

5   G.-D. Lee, C. Z. Wang, E. Yoon, N.-M. Hwang, D.-Y. Kim and K. M. Ho, *Phys. Rev. Lett.*, 2005, **95**, 205501.

6   L. M. Woods, S. C. Badescu and T. L. Reinecke, *Phys. Rev. B*, 2007, **75**, 155415.

7   M. K. Zalalutdinov, J. T. Robinson, C. E. Junkermeier, J. C. Culbertson, T. L. Reinecke, R. Stine, P. E. Sheehan, B. H. Houston and E. S. Snow, *Nano Letters*, 2012, **12**, 4212–4218.

8   D. Solenov, C. Junkermeier, T. L. Reinecke and K. A. Velizhanin, *Phys. Rev. Lett.*, 2013, **111**, 115502.

9   C. E. Junkermeier, D. Solenov and T. L. Reinecke, *The Journal of Physical Chemistry C*, 2013, **117**, 2793–2798.

10   V. Lukose, R. Shankar and G. Baskaran, *Physical Review Letters*, 2007, **98**, 116802.

11   P. Vogt, P. De Padova, C. Quaresima, J. Avila, E. Frantzeskakis, M. C. Asensio, A. Resta, B. Ealet and G. Le Lay, *Phys. Rev. Lett.*, 2012, **108**, 155501.

12   Z. Y. Ni, Q. H. Liu, K. C. Tang, J. X. Zheng, J. Zhou, R. Qin, Z. X. Gao, D. P. Yu and J. Lu, *Nano Letters*, 2012, **12**, 113–118.

13   D. Golberg, Y. Bando, Y. Huang, T. Terao, M. Mitome, C. Tang and C. Zhi, *ACS Nano*, 2010, **4**, 2979–2993.

14   D. Golberg, Y. Bando, O. Stephan and K. Kurashima, *Applied Physics Letters*, 1998, **73**, 2441–2443.

15   A. Rubio, J. L. Corkill and M. L. Cohen, *Physical Review B*, 1994, **49**, 5081–5084.

16   X. Li, X. Hao, M. Zhao, Y. Wu, J. Yang, Y. Tian and G. Qian, *Advanced Materials*, 2013, **25**, 2200–2204.

17   E. Perim and D. S. Galvao, *Nanotechnology*, 2009, **20**, 335702.

18   H. W. Kroto, J. R. Heath, S. C. Obrien, R. F. Curl and R. E. Smalley, *Nature*, 1985, **318**, 162–163.

19   V. R. Coluci, R. P. B. dos Santos and D. S. Galvao, *Journal of Nanoscience and Nanotechnology*, 2010, **10**, 4378–4383.

20   V. R. Coluci, N. M. Pugno, S. O. Dantas, D. S. Galvao and A. Jorio, *Nanotechnology*, 2007, **18**, 335702.

21   Y. Li, X. Qiu, Y. Yin, F. Yang and Q. Fan, *Physics Letters A*, 2010, **374**, 1773–1778.

22   V. R. Coluci, D. S. Galvao and A. Jorio, *Nanotechnology*, 2006, **17**, 617–621.

23   R. H. Baughman, H. Eckhardt and M. Kertesz, *The Journal of Chemical Physics*, 1987, **87**, 6687–6699.

24   M. Bieri, M. Treier, J. Cai, K. Ait-Mansour, P. Ruffieux, O. Groening, P. Groening, M. Kastler, R. Rieger, X. Feng, K. Muellen and R. Fasel, *Chemical Communications*, 2009, 6919–6921.

25   G. Brunetto, P. A. S. Autreto, L. D. Machado, B. I. Santos, R. P. B. dos Santos and D. S. Galvao, *Journal of Physical Chemistry C*, 2012, **116**, 12810–12813.

26   C. Ray, M. Pellarin, J. L. Lerme, J. L. Vialle, M. Broyer, X. Blase, P. Melinon, P. Keghelian and A. Perez, *Phys. Rev. Lett.*, 1998, **80**, 5365.

27   L. Hultman, S. Stafstrom, Z. Czigany, J. Neidhardt, N. Hellgren, I. F. Brunell, K. Suenaga and C. Colliex, *Phys. Rev. Lett.*, 2001, **87**, 225503.

28   I. Narita and T. Oku, *Diamond and Related Materials*, 2003, **12**, 1146 – 1150.

29 T. Nakamura, K. Ishikawa, A. Goto, M. Ishihara, T. Ohana and Y. Koga, *Diamond and Related Materials*, 2003, **12**, 1908 – 1911.

30 P. Melinon, B. Masenelli, F. Tournus and A. Perez, *Nat. Mater.*, 2007, **6**, 479.

31 H.-J. Zhai, Y.-F. Zhao, W.-L. Li, Q. Chen, H. Bai, H.-S. Hu, Z. A. Piazza, W.-J. Tian, H.-G. Lu, Y.-B. Wu, Y.-W. Mu, G.-F. Wei, Z.-P. Liu, J. Li, S.-D. Li and L.-S. Wang, *Nature chemistry*, 2014, **6**, 727–731.

32 G. Otero, G. Biddau, C. Sanchez-Sanchez, R. Caillard, M. F. Lopez, C. Rogero, F. J. Palomares, N. Cabello, M. A. Basanta, J. Ortega, J. Mendez, A. M. Echavarren, R. Perez, B. Gomez-Lor and J. A. Martin-Gago, *Nature*, 2008, **454**, 865.

33 M. Elstner, D. Porezag, G. Jungnickel, J. Elsner, M. Haugk, T. Frauenheim, S. Suhai and G. Seifert, *Physical Review B*, 1998, **58**, 7260–7268.

34 A. C. T. van Duin, S. Dasgupta, F. Lorant and W. A. Goddard, *Journal of Physical Chemistry A*, 2001, **105**, 9396–9409.

35 Y. Ding, Y. Wang, S. Shi and W. Tang, *Journal of Physical Chemistry C*, 2011, **115**, 5334–5343.

36 K. Balasubramanian, *Journal of Physical Chemistry*, 1993, **97**, 6990–6998.

37 D. Bruns, H. Miura, K. P. C. Vollhardt and A. Stanger, *Organic letters*, 2003, **5**, 549–552.

38 A. Balaban, *Theoretical and Computational Chemistry*, 1998, **5**, 381–404.

39 Y. Ding, Y. Wang, S. Shi and W. Tang, *J. Phys. Chem. C*, 2011, **115**, 53345343.

40 H. Manzano, A. N. Enyashin, J. S. Dolado, A. Ayuela, J. Frenzel and G. Seifert, *Advanced Materials*, 2012, **24**, 3239–3245.

41 T. Kubar, Z. Bodrog, M. Gaus, B. Koehler, B. Aradi, T. Frauenheim and M. Elstner, *Journal of Chemical Theory and Computation*, 2013, **9**, 2939–2949.

42 M. V. Diudea, A. Bende and C. L. Nagy, *Phys. Chem. Chem. Phys.*, 2014, **16**, 5260–5269.

43 B. Lukose, A. Kuc, J. Frenzel and T. Heine, *Beilstein J Nanotechnol.*, 2010, **1**, 60–70.

44 A. C. T. van Duin and J. S. S. Damste, *Organic Geochemistry*, 2003, **34**, 515–526.

45 K. Chenoweth, A. C. T. van Duin and I. Goddard, William A., *Journal of Physical Chemistry A*, 2008, **112**, 1040–1053.

46 N. L. Allinger, Y. H. Yuh and J. H. Lii, *Journal of the American Chemical Society*, 1989, **111**, 8551–8566.

47 J. H. Lii and N. L. Allinger, *Journal of the American Chemical Society*, 1989, **111**, 8566–8575.

48 A. Shekhar, K. Nomura, R. K. Kalia, A. Nakano and P. Vashishta, *Physical Review Letters*, 2013, **111**, 184503.

49 M. R. Weismiller, A. C. T. v. Duin, J. Lee and R. A. Yetter, *The Journal of Physical Chemistry A*, 2010, **114**, 5485–5492.

50 S. Plimpton, *Journal of computational physics*, 1995, **117**, 1–19.

51 P. Kowalczyk and R. Holyst, *Environmental science & technology*, 2008, **42**, 2931–2936.

52 O. O. Adisa, B. J. Cox and J. M. Hill, *Physica B: Condensed Matter*, 2011, **406**, 88–93.

53 J. H. Yang, D. H. Lee, M. H. Yum, Y. S. Shin, E. J. Kim, C.-Y. Park, M. H. Kwon, C. W. Yang, J.-B. Yoo, H.-J. Song *et al.*, *Carbon*, 2006, **44**, 2219–2223.

54 S. Legoas, R. Dos Santos, K. Troche, V. Coluci and D. Galvao, *Nanotechnology*, 2011, **22**, 315708.

55 A. N. Khlobystov, D. A. Britz, A. Ardavan and G. A. D. Briggs, *Phys. Rev. Lett.*, 2004, **92**, 245507.